Supplemental Information

Enhanced Reliability of Phase-change Memory Through Modulation of Local Structure and Chemical Bond by Carbon Incorporation into Ge$_2$Sb$_2$Te$_5$

Jeong Hwa Han[1,†]*, Hun Jeong*[1,†]*, Hanjin Park*[2,†]*, Hoedon Kwon*[1]*, Dasol Kim*[1]*, Donghyeok Lim*[,3]*, Seung Jae Baik*[4]*, Young-Kyun Kwon*[2,5*]*, and Mann-Ho Cho*[1,6,*]

[1]Department of Physics, Yonsei University, Seoul 03722, Republic of Korea

[2]Department of Physics and Research Institute for Basic Sciences, Kyung Hee University, Seoul 02447, Republic of Korea

[3]Department of Materials Science and Engineering, UNIST, Ulsan 44919, Republic of Korea

[4]Faculty of Electronic and Electrical Engineering, Hankyong National University, Anseong 17579, Republic of Korea

[5]Department of Information Display, Kyung Hee University, Seoul 02447, Republic of Korea

[6]Department of System Semiconductor Engineering, Yonsei University, Seoul 03722, Republic of Korea

[*]Corresponding authors: E-mail: ykkwon@khu.ac.kr, mh.cho@yonsei.ac.kr
[†]These authors contributed equally to this work.

Table S1. Raman peaks in Figure 2, marked as A–E, for the as-grown film are compared with those for the re-amorphized film. The value of each peak area is listed in this table. The basic information for structural ratio summarized in Table 1 can be derived using these values.

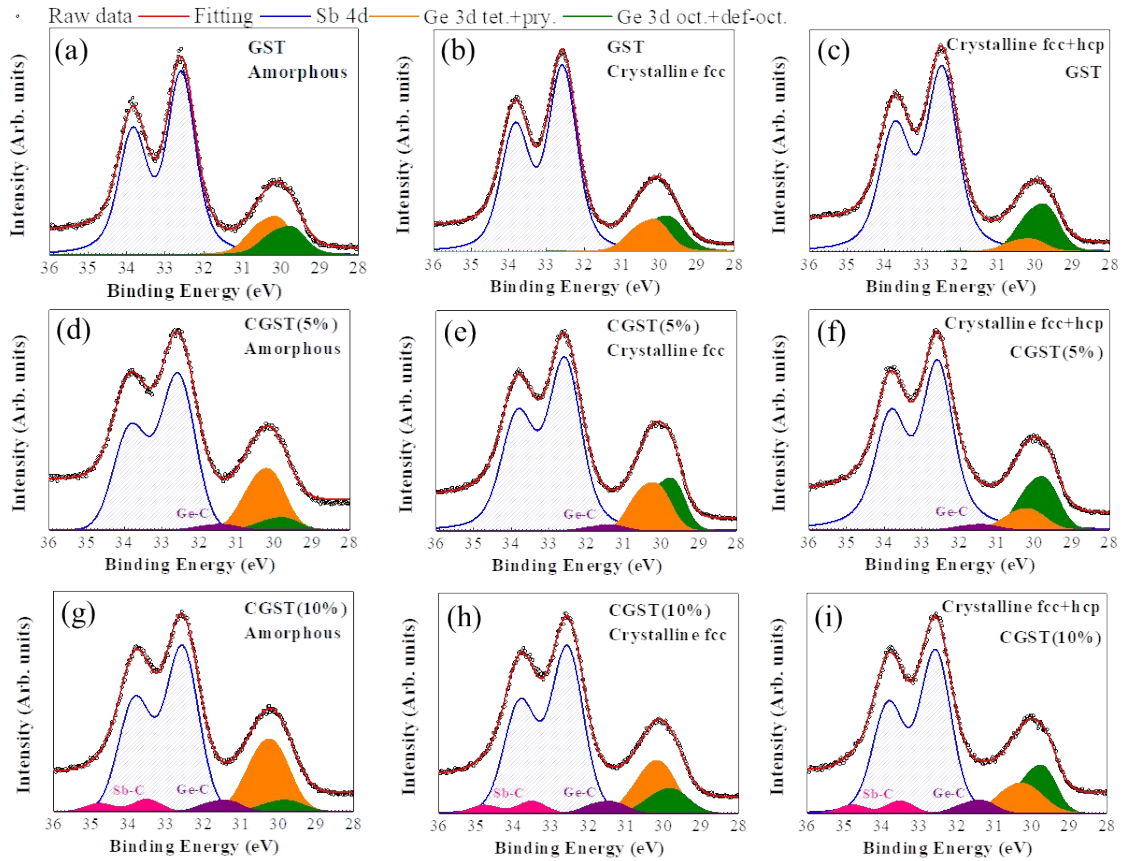|	GST	Reamorphized GST	CGST(5%)	Reamorphized CGST(5%)	CGST(10%)	Reamorphized CGST(10%)
A	3167	3396	3327	3992	4095	4170
B	1343	903	1105	653	1539	968
C	4131	3909	4584	5478	6051	7740
D	11666	15159	13469	15640	12946	12049
E	569	1022	529	689	1321	1321

Figure S1. In situ XPS results of Ge 3d and Sb 4d peaks with incorporated C. The modulation of the chemical bonding state caused by the structural change is observed; specifically, Ge$^{tet + pyr}$ further decreases and Ge$^{oct + def\text{-}oct}$ further increases with the C content in CGST than those in GST.

In general, the change in chemical bonding with Ge represents the structural modulation in GST between the tetrahedral and octahedral structures during the phase change process, as shown in Figure S1. Through the deconvolution process and by using the reported data for the tetrahedral, pyramidal, octahedral, and defective octahedral structures, we attempted to deconvolute Ge 3d peak into four sub-peaks. However, the peak could not be successfully deconvoluted due to the energy resolution limit in the measurement system. Moreover, the reported difference in the bonding energies between the octahedral and defective octahedral (or tetrahedral and pyramidal) structures is extremely small; hence, it cannot detect this deviation despite the use of an in situ measurement system. Although the Ge 3d peak could not be deconvoluted into each sub-peak of the four different structures, the observed peaks could be distinguished by two sub-peaks. In particular, one sub-peak corresponds to the amorphous structure for the tetrahedral and pyramidal structures (Ge$^{tet + pyr}$). The other sub-peak is associated with

3

the crystalline structure for the octahedral and defective octahedral structures ($Ge^{oct+def-oct}$). This finding well agrees with the structural change that occurs during the transition between the amorphous and crystalline phases.
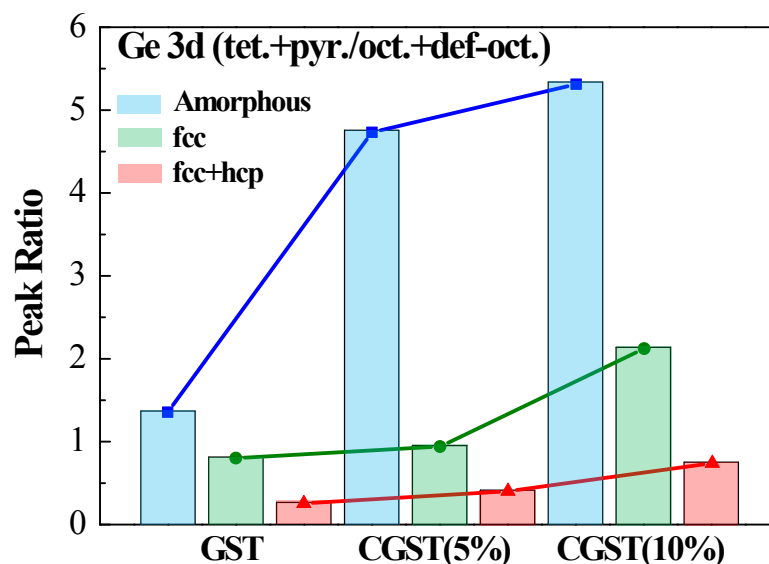

Figure S2. Ge 3d peak ratio of amorphous (tetrahedral and pyramidal) structures to crystalline (octahedral and defective octahedral) structures can be expressed by a formula. The modulation of the chemical bonding state caused by the incorporated C is observed; specifically, $Ge^{tet+pyr}$ further increases and $Ge^{oct+def-oct}$ further decreases with the content of C in CGST than those in GST.

$Ratio = (tetrahedral + pyramidal) \div (octahedral + defective\ octahedral)$

The formula was derived from the peak in situ XPS results in Figure S1. The Ge 3d peak ratio of the amorphous (tetrahedral and pyramidal) structures to crystalline (octahedral and defective octahedral) structures, i.e., $(Ge_{tet.+pyr.})/(Ge_{oct.+def-oct.})$, is determined to investigate the dependence of the incorporated carbon content on the crystal structure, as shown in the aforementioned figure. The value shows clear dependence on the incorporated carbon content. That is, consistent with the Raman data, the carbon content increases with the peak area of $(Ge_{tet.+pyr.})$ in the amorphous state. Although the value significantly decreases after the phase change to the crystalline structure, it remains higher than that in GST. Moreover, a distinct difference in the peak ratio between 5% and 10% CGSTs is observed. In 10%

CGST, the local portion for the (tetrahedral + pyramidal) structure as the 2nd stable local structure is considerably more than that for the (octahedral + defective octahedral) structure as the 1st stable local structure after the phase change from the amorphous state to the fcc structure. The portion for the (tetrahedral + pyramidal) structure finally decreases to less than that for the (octahedral + defective octahedral) structure after the subsequent phase change from the fcc to hcp structure. The decrease in the portion of the crystallized region in CGST at the same annealing temperature compared with that in GST indicates that the crystallization from the amorphous phase to the fcc structure and from the fcc to hcp structure is effectively hindered in CGST. Additionally, we confirmed that the peak intensity for the chemical states of C bonded with Sb and Ge increased with the C content. Consistent with reported data, the Ge–C bond with bonding energy of 31.45 eV is formed at a low C content. A new Sb–C bond with a bonding energy of 34 eV is observed at a high C content, suggesting that the bond is possibly closely related to the difference in structure and resistivity between the samples with high and low C contents.
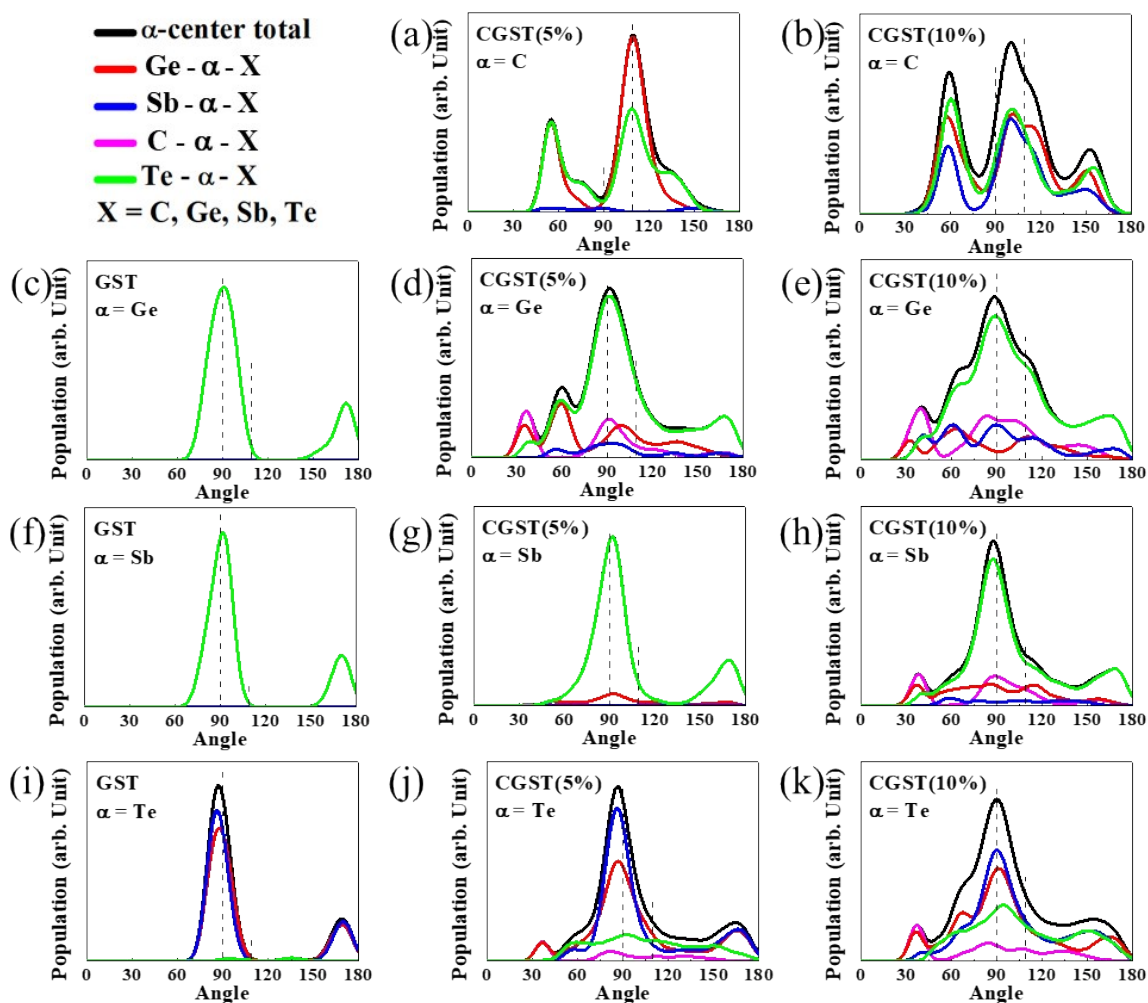
Figure S3. Representation of angular distribution function (ADF) of the full dataset. The modulation of the bonding angle of atoms caused by the change in the chemical bond of the incorporated carbon was investigated by the ADF. The data for every atom from the constant-temperature MD simulation were used to evaluate the ADF.

To analyze the local environment of CGST, a constant-temperature molecular dynamics (MD) simulation was implemented. The classical Newton equation of motion was solved with the quantum mechanical force acting on each atom calculated by the Hellmann–Feynman theorem. The constant temperature was maintained using the Nosé thermostat with a heat bath temperature of 300 K. The necessary data for every atom during the 4.5-ps MD simulation were collected and used to evaluate the ADF.
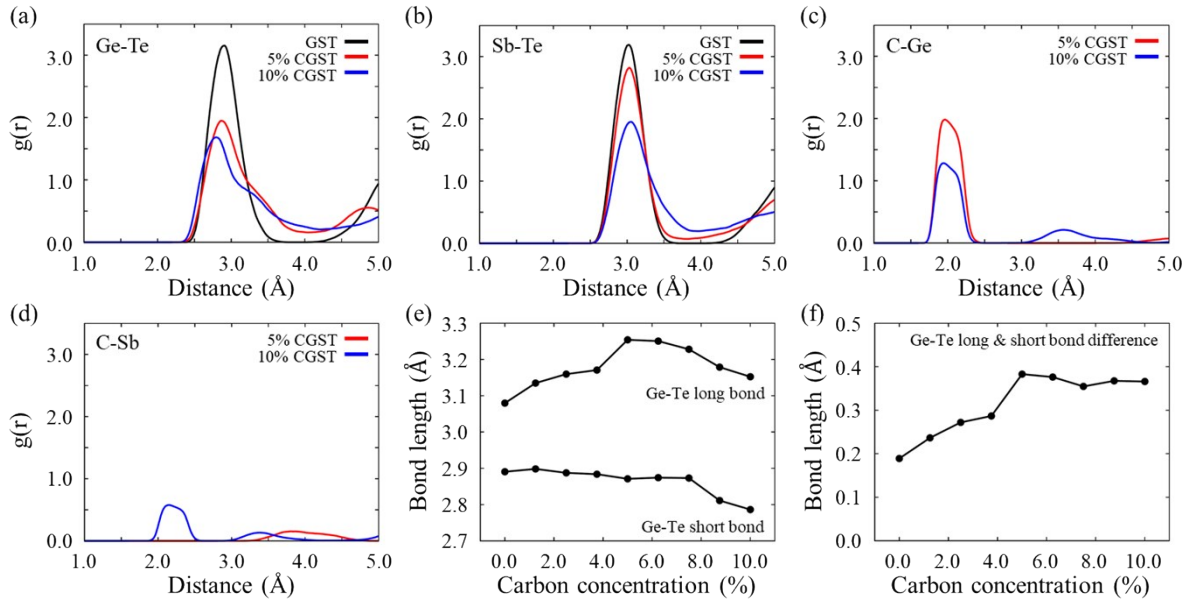
Figure S4. Radial distribution function, g(r), representing the variation in the radial distribution of chemical bonding distance between two atoms: (a) Ge–Te, (b) Sb–Te, (c) C–Ge, and (d) C–Sb. (e) Change in the Ge–Te bond length with carbon content; (f) difference in the Ge–Te bond length between long and short bonds according to carbon content.

The distances between the Ge–Te and Sb–Te atoms are confirmed through Figure S4, (a)–(c), and Table S2; their values slightly vary. To further verify the modulation of the bonding formation due to the incorporated carbon, the radial distribution function is implemented. In the figure, g(r) represents the variation in the radial distribution of chemical bonding between two atoms. Similar to reported data, only the Ge–C bond exists in CGST with low C content (<5%). However, in CGST with high C content (~10%), the Sb–C bond forms and its length increases depending on the incorporated C content. This is consistent with the XPS experimental data for Sb–C bond formation. These results strongly suggest that the chemical bonding caused by the incorporated carbon affects structural distortion.

Table S2. Fitting parameters and average coordination numbers from the Ge K-edge X-ray absorption spectra of GST and the 5% and 10% CGST films. The EXAFS data were analyzed with the FEFF8 code using an optimized structure, and the structural parameters were optimized using ARTEMIS.

	GST	CGST(5%)	CGST(10%)
	Ge-Te	Ge-Te	Ge-Te
R	2.83 Å	2.77 Å	2.81 Å
N	2.40	3.34	3.17
σ^2	0.012 ± 0.0039	0.016 ± 0.0016	0.022 ± 0.0059

.

Table S3. Equation of the reset energy of GST and 5% and 10% CGST devices is derived as $E_{reset} = (V^2_{reset}/R_{set}) \times t_{reset}$. The reset energy of 5% CGST (~0.2 nJ) increases more than twice that of GST (~0.1 nJ). When the carbon content in CGST is doubled (i.e., 10%), the reset energy slightly increases

Reset Energy [nJ]		
GST	CGST(5%)	CGST(10%)
0.098	0.204	0.216

to ~0.21 nJ compared with that in 5% CGST.